

# MVLoc: Multimodal Variational Geometry-Aware Learning for Visual Localization

Rui Zhou<sup>1</sup>, Changhao Chen<sup>1</sup>, Bing Wang<sup>1</sup>, Andrew Markham<sup>1</sup>, and Niki Trigoni<sup>1</sup>

Department of Computer Science, University of Oxford, UK  
`{firstname.lastname}@cs.ox.ac.uk`

**Abstract.** Recent learning-based research has achieved impressive results in the field of single-shot camera relocation. However, how best to fuse multiple modalities, for example, image and depth, and how to deal with degraded or missing input are less well studied. In particular, we note that previous approaches towards deep fusion do not perform significantly better than models employing a single modality. We conjecture that this is because of the naive approaches to feature space fusion through summation or concatenation which do not take into account the different strengths of each modality, specific appearance for images and structure for depth. To address this, we propose an end-to-end framework to fuse different sensor inputs through a variational Product-of-Experts (PoE) joint encoder followed by attention-based fusion. Unlike prior work which draws a single sample from the joint encoder, we show how accuracy can be increased through importance sampling and reparameterization of the latent space. Our model is extensively evaluated on RGB-D datasets, outperforming existing baselines by a large margin.

**Keywords:** Visual Localization, Variational Inference, Multimodal Learning

## 1 Introduction

Visual localization is of great importance to many intelligent systems, e.g. autonomous vehicles, delivery drones, and virtual reality (VR) devices. Recently, deep learning has shown its strengths in learning camera pose from raw images in an end-to-end manner. However, when deployed in complex and ever-changing real-world environments, a single modality solution is normally confronted with real issues, such as environmental dynamics, changes in lighting conditions and extreme weather. Meanwhile, those intelligent systems are generally equipped with a combination of sensors (e.g. cameras, depth sensors, and LIDAR).

Current studies concentrating on sensor fusion always directly concatenates different features vector together before following operations, e.g., [23, 1], without studying the information contained in different feature vectors. Effectively exploiting different sensor modalities and studying their complementary features

will contribute to a more accurate and robust localization system. Compared with localization algorithms using only RGB images, e.g. PoseNet [19], Bayesian PoseNet [16], Hourglass Network [25], CNN+LSTM localization neural network [34], PoseNet17 [17], etc., multimodal localization is far less to be explored.

Although there are advances in multimodal learning [31,14,37] and learning based sensor fusion strategies [21,26,33], few of them investigate the strategies for visual localization. How to exploit the multiple sensor modalities to achieve accurate pose estimation is an important step to developing robust intelligent systems. To address this, we propose MVLoc (**M**ultimodal **V**ariational **L**ocalization), a novel framework to learn multimodal localization. The key component of this framework is our proposed MVGAL (**M**ultimodal **V**ariational **G**eometry-Aware **L**earning) that learns a joint latent representation from a pair of sensor modalities, i.e. vision and depth data, or LIDAR and vision data. Our work is most related with VidLoc [9] and MVAE [37]. VidLoc [9] simply concatenates RGB image and depth map, and processes them together with convolutional neural networks (CNN) for camera relocalization. However, this direct concatenation on the raw data level won't take advantage of the complementary properties of different data. Instead, we provide systematic research into the fusion strategy of the visual localization task, and our method outperforms previous localization methods. MVAE [37] proposes to use variational inference to learn an invariant space from multimodal fusion, and achieved impressive results in several tasks. However, it is hard to scale to real-world environments with high-dimensional raw images and rich scene information. We further incorporate the importance weighting strategy and geometric learning to enable the framework to learn useful representations from data.

Our work focuses on the problem fusing a pair of modalities, although it can be easily extended to multiple modalities without significantly increasing the computational burden. Our intuition is that there should exist a common space from multiple sensor modalities, that is useful and suitable for solving the task at hand. As Figure 2 demonstrates, our fusion approach learns a joint latent representation of different modalities and then regress 6-DoF pose estimation. The individual latent spaces of each modality are combined by the Product-of-Experts (PoE), allowing each modality to concentrate on the specific property of the data. This model can be trained in an end-to-end manner. The main contributions of this work can be summarized as follow:

- We propose MVGAL, a novel variational multimodal fusion strategy, that effectively exploits different data modalities and learns a joint latent space.
- Based on MVGAL, we introduce MVLoc, a deep neural network framework to combine a pair of sensor modalities, e.g. vision and depth, or LIDAR and vision for pose regression.
- Extensive experiments on indoor and outdoor scenarios and a systematic research into the robustness and ablation demonstrate the effectiveness of our proposed framework, outperforming previous visual localization work.

## 2 Related Work

### 2.1 Sensor Fusion and Multimodal learning

Because of the complementary properties of different sensors, an effective and suitable fusion strategy plays a vital role in learning from multiple sensor modalities. However, the distinctive characteristics of heterogeneous sensor data make the task of sensor fusion complicated. To date, limited research has considered sensor fusion in the context of visual localization. [2] analyzes localization performance using three kinds of sensors including a laser rangefinder, a depth camera, and WiFi. Specifically, they identify the sensor which can provide the most accurate location estimation in different situations. [6] proposes an end-to-end selective fusion framework for monocular VIO which fuses monocular images and inertial measurements to estimate the trajectory which can, to some extent, solve the corrupted input problem. Nevertheless, their performances are still very limited and they couldn't provide better result than state-of-the-art based on only monomodality.

Moreover, learning a joint representation and studying the respective contribution from different modalities are also the focus of multi-modal learning. Among them, some works propose to learn an explicit joint distribution of all modalities. [31] proposes a joint multi-modal variational auto-encoder (JMVAE) to extract a joint representation among all models, in which all modalities are independently conditioned on the joint representation; [37] uses a PoE inference network and a sub-sampled training paradigm to learn a joint representation and to solve the multi-modal inference problem. However, both of JMVAE and PoE are only tested in simple datasets, e.g., MNIST [22], Fashion MNIST [38], etc. Their performances are doubtful when dealing with more complicated real-life tasks.

Other works propose to learn the individual subspace and to achieve cross inference among modalities. For example, [29] proposes a mixture-of-experts (MoE) multimodal variational autoencoder (MMVAE) to learn the individual latent space of each modality and realizes the cross-modal generation; [14] introduces the symbol-concept association network(SCAN), which minimizes the KL divergence between different latent spaces and deals with the multimodal bi-directional inference task. Compared with them, our work introduces importance weighting strategy into the multimodal variational model to improve its modelling capacity and to reduce the training variance. Meanwhile, we incorporate the geometric loss into the inference process to encourage useful features for pose estimation.

### 2.2 Camera Localization via Deep Learning

Instead of basing on 3D-geometry theory to tackle the problem [7,11,40], deep learning models directly learn useful features from raw data [27,34] to regress 6-DoF pose. PoseNet [19] first leveraged convolutional neural networks to learn

and predict camera poses from single images. Subsequently, the PoseNet structure was further developed to enhance the performance, e.g. the skip connection introduced in [25]. Besides architectural refinements, the loss function used in the optimization can also be enhanced. Instead of using the combination of position and rotation errors and in the training process [18,34], visual odometry constraints [3] are incorporated to improve the model performance; [17] proposed using a learning weighted loss and a geometric re-projection loss to generate the more accurate result. Furthermore, the use of recurrent neural network has been introduced to improve the localization accuracy from both the temporal aspect [10] and the spatial aspect [34]. To date, deep relocalization has largely considered a single modality as input. However, our work proposes a fusion framework that can effectively use the data from several different sensors to solve the camera localization problem.

### 3 Multi-modal Variational Visual Localization

#### 3.1 Problem Formulation

This work is aimed at exploiting multimodal data to achieve more robust and accurate pose estimation  $\mathbf{y} = (\mathbf{p}, \mathbf{q})$ , which consists of a location vector  $\mathbf{p} \in \mathbb{R}^3$  and a quaternion based orientation vector  $\mathbf{q} \in \mathbb{R}^4$ . The multimodal data are the different observations of an identical scene, but complementary to each other, e.g. RGB images contain the appearance and semantic information of a scene, while depth maps or point cloud data capture the scene structure. Intuitively, these sensor modalities all reflect a spatial sense of this scene, and hence a common feature space should exist.

Given two sensor modalities  $\mathbf{x}^1$  and  $\mathbf{x}^2$ , we aim to learn their joint latent representation  $\mathbf{z}$ . As shown in Figure 1, this problem is formulated as a Bayesian inference model, which is to maximize the posterior probability conditioned on input data:

$$\mathbf{z} = \underset{\mathbf{z}}{\operatorname{argmax}}[p(\mathbf{z}|\mathbf{x}^1, \mathbf{x}^2)]. \quad (1)$$

Based on this intermediate representation  $\mathbf{z}$ , the target value  $\mathbf{y}$  is obtained by

$$\mathbf{y} = \underset{\mathbf{y}}{\operatorname{argmax}}[p(\mathbf{y}|\mathbf{z})]. \quad (2)$$

The problem becomes how to recover the joint distribution of two modalities. Our work mainly considers a pair of modalities, although the proposed method can be naturally extended to the usage of three or more modalities.

#### 3.2 Multimodal Variational Geometry-Aware Learning

We introduce MVGAL (Multimodal Variational Geometry-Aware Learning) framework to tackle this multimodal learning problem. Our proposed method leverages the variational inference models [20] to find a distribution  $q_\phi(\mathbf{z}|\mathbf{x}^1, \mathbf{x}^2)$ , approximating the true posterior distribution  $p(\mathbf{z}|\mathbf{x}^1, \mathbf{x}^2)$  with the aid of the corresponding geometric information. Table 1 demonstrates the detailed algorithmic description of our proposed MVGAL.

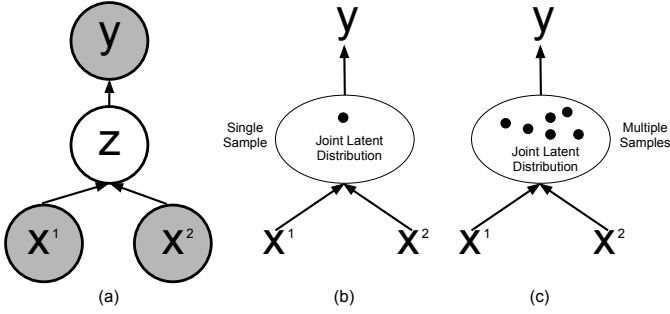


**Fig. 1.** (a) The graphical model of our proposed MVLoc method. (b) In the standard variational inference, e.g. MVAE, the representation is only resampled once from the distribution. (c) We introduce the importance weighting technique in the multimodal variational inference to enhance the modelling capacity.

**Multimodal Variational Inference** Unlike conventional variational autoencoders (VAE) [20], MVGAL reconstructs a target value  $\mathbf{y}$  in a different domain, i.e. 6-DoF pose in our case, instead of the original domain data. Similar to the cross-modality VAE [39], MVGAL produces the target value  $\mathbf{y}$  via a joint latent variable  $\mathbf{z}$  of two modalities  $\mathbf{x}^1$  and  $\mathbf{x}^2$ , by maximizing the evidence-lower-bound (ELBO) as follow:

$$\begin{aligned} \log p(\mathbf{y}) &\geq \mathbb{E}_{\mathbf{z} \sim q_{\phi}(\mathbf{z}|\mathbf{x}^1, \mathbf{x}^2)} [\log \frac{p_{\theta}(\mathbf{y}|\mathbf{z})p(\mathbf{z})}{q_{\phi}(\mathbf{z}|\mathbf{x}^1, \mathbf{x}^2)}] \\ &= \text{ELBO}(\mathbf{y}; \mathbf{x}^1, \mathbf{x}^2) \end{aligned} \quad (3)$$

where  $p(\mathbf{y})$  is the distribution of target value,  $p(\mathbf{z})$  is the prior distribution of latent space,  $q_{\phi}(\mathbf{z}|\mathbf{x}^1, \mathbf{x}^2)$  is the inference model to approximate the posterior distribution  $p(\mathbf{z}|\mathbf{x}^1, \mathbf{x}^2)$ , and  $p_{\theta}(\mathbf{y}|\mathbf{z})$  is the decoder network.

Inspired by MVAE [37], the inference problem of  $p(\mathbf{z}|\mathbf{x}^1, \mathbf{x}^2)$  can be simplified as learning two conditional distributions  $p(\mathbf{z}|\mathbf{x}^1)$  and  $p(\mathbf{z}|\mathbf{x}^2)$  separately. This is under the assumption that two modalities are conditionally independent given the latent representation. Based on that, we can apply the product-of-experts (PoE) technique to estimate the joint latent distribution  $p(\mathbf{z}|\mathbf{x}^1, \mathbf{x}^2)$  via:

$$p(\mathbf{z}|\mathbf{x}^1, \mathbf{x}^2) = \frac{p(\mathbf{z}|\mathbf{x}^1)p(\mathbf{z}|\mathbf{x}^2)}{p(\mathbf{z})}. \quad (4)$$

Here, PoE works to combine several simple distributions by producing their density functions [15]. In our case, it allows each modality to specialize in their specific property to contribute to the final pose estimation, rather than forcing each modality to recover the full-dimensional information to solve problem.

As the distribution  $p(\mathbf{z}|\mathbf{x}^1)$  can be approximated with an inference network  $q(\mathbf{z}|\mathbf{x}^1) \equiv \tilde{q}(\mathbf{z}|\mathbf{x}^1)q(\mathbf{z})$ , Equation 4 is further developed as

$$p(\mathbf{z}|\mathbf{x}^1, \mathbf{x}^2) = \tilde{q}(\mathbf{z}|\mathbf{x}^1)\tilde{q}(\mathbf{z}|\mathbf{x}^2)q(\mathbf{z}). \quad (5)$$

Thus the learning process can be summarized as: it first learns two individual latent distributions  $p(\mathbf{z}|\mathbf{x}^1)$  and  $p(\mathbf{z}|\mathbf{x}^2)$ ; then combines two distributions to obtain the final joint distribution. In practice, we assume that both the prior distribution and the posterior distribution are the Gaussian distributions. With the mean vector and the variance matrix, we can sample from the learned distribution to get the joint latent representation of inputted modalities.

**Importance Weighting Strategy** However, directly optimizing ELBO as the objective function can only provide simplified representation. As shown in Figure 1 (b), in the normal variational model, e.g. MVAE, the representation is only resampled once from the latent distribution. In this way, the capability of variational inference has not been fully exploited and our latter experiments support this argument. Therefore, we introduce the importance weighting strategy into the framework. As Figure 1 (c) illustrates, instead of only depending on one sample, this strategy resamples from learned distribution for multiple times to approximate the posterior distribution, which allows network to model more complicated posterior distribution. In doing so, it provides a strictly tighter log-likelihood lower bound [5] through:

$$\mathbb{E}[\log \frac{1}{k} \sum_{i=1}^k w_i] \geq \mathbb{E}[\log \frac{1}{k-1} \sum_{i=1}^{k-1} w_i], \quad (6)$$

where  $w_i = p(\mathbf{y}, \mathbf{z}_i)/q(\mathbf{z}_i|\mathbf{x}^1, \mathbf{x}^2)$ ;  $k$  is the number of samples;  $\mathbf{z}_i$  is the  $i$ th point sampled independently from the latent distribution. Thus, the objective function is rewritten as:

$$\begin{aligned} \log p(\mathbf{y}) &= \log \mathbb{E}[w] \\ &\geq \mathbb{E}[\log \frac{1}{k} \sum_{i=1}^k w_i] \\ &= \text{ELBO}(\mathbf{y}; \mathbf{x}^1, \mathbf{x}^2). \end{aligned} \quad (7)$$

It can be noticed from above analysis, that the larger number of samples leads to tighter log-likelihood lower bound. With this new objective function, our model uses multiple samples instead of one to approximate the posterior, which improve its capability to learn more complex posterior.

Although, by increasing the number of samples, we are able to find a tighter bound, it counter-intuitively leads to a higher variance for gradient estimation in the training process [28]. The gradients of the objective function in Equation 7 are calculated via:

$$\nabla_{\phi} L_k = \mathbb{E}_{\varepsilon_{1:k}} [\sum_{i=1}^k w_i \frac{w_i}{\sum_j w_j} (\frac{\partial \log w_i}{\partial \mathbf{z}_i} \frac{\partial \mathbf{z}_i}{\partial \phi} - \frac{\partial}{\partial \phi} \log q_{\phi}(\mathbf{z}_i|\mathbf{x}^1, \mathbf{x}^2))]. \quad (8)$$

According to [28], the second item (score function) in Equation 8 can be eliminated, so as to reduce the variance of the gradients. However, they fail to show

that eliminating this item is unbiased. To address this concern, [32] eliminates the score function by rewriting Equation 8 as:

$$\nabla_{\phi} L_k = \mathbb{E}_{\varepsilon_{1:k}} \left[ \sum_{i=1}^k \left( \frac{w_i}{\sum_j w_j} \right)^2 \frac{\partial \log w_i}{\partial \mathbf{z}_i} \frac{\partial \mathbf{z}_i}{\partial \phi} \right]. \quad (9)$$

Through Equation 9, we mitigate the side effects of increasing  $k$  and ensure the gradients of the inference network are unbiased.

Instead of directly computing  $w_i = p(\mathbf{y}, \mathbf{z}_i) / q(\mathbf{z}_i | \mathbf{x}^1, \mathbf{x}^2)$  as in Equation 9, in practice, we rewrite it as follow:

$$\begin{aligned} w_i &= e^{\log w_i} \\ &= e^{\log p(\mathbf{y}|\mathbf{z}_i) + \log p(\mathbf{z}_i) - \log(q(\mathbf{z}_i|\mathbf{x}^1, \mathbf{x}^2))} \end{aligned} \quad (10)$$

We further replace the first logarithm likelihood item in Equation 10 with the negative geometric loss which calculates the distance between the predicted pose and the target pose in the pose estimation task.

**Geometric Learning** To encourage MVGAL to extract useful features for pose estimation, we propose to incorporate geometric information into the optimization objective. We incorporate a learnable geometric loss [10,4] into the loss function:

$$L_p(\mathbf{y}, \mathbf{y}^*) = \|\mathbf{p} - \mathbf{p}^*\| e^{-\beta} + \beta + \|\log \mathbf{q} - \log \mathbf{q}^*\| e^{-\gamma} + \gamma \quad (11)$$

where  $\mathbf{y}^* = (\mathbf{p}^*, \mathbf{q}^*)$  is the ground truth pose, while the  $\beta$  and the  $\gamma$  are the weights that balance the position loss and the rotation loss. The  $\beta$  and the  $\gamma$  are optimized during the training process with the initial value  $\beta_0$  and  $\gamma_0$ . The  $\log \mathbf{q}$  is the logarithmic form of a unit quaternion  $\mathbf{q}$ , which is defined as:

$$\log \mathbf{w} = \begin{cases} \frac{\mathbf{v}}{\|\mathbf{v}\|} \cos^{-1} \mathbf{u}, & \text{if } \|\mathbf{v}\| \neq 0 \\ \mathbf{0}, & \text{otherwise} \end{cases} \quad (12)$$

where  $\mathbf{u}$  denotes the real part of a unit quaternion and  $\mathbf{v}$  is the imaginary part [35]. In general, the gradient for the inference network  $\phi$  and the decoder network  $\theta$  (also known as the pose regression network) can be expressed as follow:

$$\begin{aligned} \nabla_{\phi, \theta} L_k &= \mathbb{E}_{\varepsilon_{1:k}} \left[ \sum_{i=1}^k \left( \frac{w_i}{\sum_j w_j} \right)^2 \frac{\partial \log w_i}{\partial \mathbf{z}_i} \frac{\partial \mathbf{z}_i}{\partial \phi, \theta} \right]; \\ \text{where } w_i &= e^{-L_p(\mathbf{y}, \mathbf{y}^*) + \lambda (\log p(\mathbf{z}_i) - \log(q(\mathbf{z}_i | \mathbf{x}^1, \mathbf{x}^2)))}, \end{aligned} \quad (13)$$

where  $\lambda$  is the hyperparameter introduced by [13] to balance the prediction accuracy and the latent space capability. The learning algorithm can be found in Algorithm 1.

---

**Algorithm 1** MVGAL algorithm
 

---

 Require:  $\mathbf{x}^1$ ,  $\mathbf{x}^2$  and  $\mathbf{y}$ 

 Initialize parameters  $\phi_{\mathbf{x}^1}$ ,  $\phi_{\mathbf{x}^2}$ ,  $\theta$ ,  $\beta$  and  $\gamma$ 
**for** episode=1,  $N$  **do**

   Encoder  $\mathbf{x}^1$  and  $\mathbf{x}^2$  with  $q_{\phi_{\mathbf{x}^1}}(\mathbf{z}|\mathbf{x}^1)$  and  $q_{\phi_{\mathbf{x}^2}}(\mathbf{z}|\mathbf{x}^2)$ 

Compute the joint distribution via Equation 5

   Sample  $k$  points  $\mathbf{z}_i$  from joint distribution

   Decode  $\mathbf{z}_i$  with  $p_{\theta}(\mathbf{y}|\mathbf{z})$ 

   Update the parameters  $\beta$  and  $\gamma$  with loss function  $L_p(\mathbf{y}, \mathbf{y}^*)$  in Equation 11

   Update the parameters  $\phi_{\mathbf{x}^1}$ ,  $\phi_{\mathbf{x}^2}$  and  $\theta$  with gradient  $\nabla_{\phi, \theta} L_k$  in Equation 13

**end for**


---

### 3.3 Framework

Now we come to introduce the framework of our proposed approach with the application on visual localization, MVLoc (**M**ultimodal **V**ariational **V**isual **L**ocalization). Figure 2 illustrates the structure of proposed MVLoc, including an RGB image encoder, a depth map encoder, an MVGAL fusion module, an attention module, and a pose regressor. These two encoders separately encode the RGB images and the depth maps into their own latent space, followed by fusing the multiple individual latent spaces into one joint latent space through MVGAL. Then the latent representation sampled from the joint latent space is re-weighted by a self-attention module. Finally, the re-weighted latent features are taken as the input for the successive pose regressor to predict the 6-DoF camera pose.

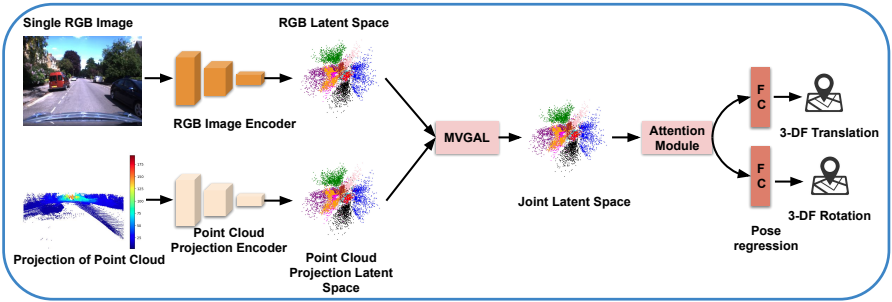


**Fig. 2.** Our framework consists of feature encoders, a MVGAL fusion module, an attention mechanism module and a pose regressor.

**Feature Encoders** The feature encoders in our framework include an image encoder  $q_{\phi_{img}}(\mathbf{z}|\mathbf{x}_{img})$  and a depth encoder  $q_{\phi_{dep}}(\mathbf{z}|\mathbf{x}_{dep})$ , which separately learn



the latent distribution of RGB image and that of depth map. In learning point-cloud feature, we transform the LIDAR pointcloud data into a depth map using the cylindrical projection [8]. Convolutional Neural Network (CNN) has already shown its strengths in the task of visual localization [4]. Among them, the ResNet model has been widely applied in different work, e.g., [4,35], and achieved the state-of-the-art performance. Based on these concerns, in our model, we also adopt the ResNet34 structure to construct our RGB image encoder and depth map encoder. To accelerate the convergence speed, the ResNet34 in our model was initialized by the weights of model trained on the Image-Net[12]. For the depth map encoder, the first convolution layer with three channels can be replaced by the convolution layer with one channel according to the dimension of depth map. For both image encoder and the depth map encoder, the second last average pooling layer is replaced by the adaptive average pooling layer and is followed by two parallel fully connected layers with the same dimension  $D$ , which separately output the mean vector  $\boldsymbol{\mu} \in \mathbb{R}^D$  and the diagonal vector of the variance matrix  $\boldsymbol{\sigma} \in \mathbb{R}^D$  of the learned latent distribution.

**MVGAL Fusion Module** After we learned the mean vector and the variance matrix for the latent distribution of the RGB image and the depth map, we compute corresponding parameters for the joint distribution via Equation 5. Rather than directly sampling from the joint distribution which isn't differentiable, the reparameterization trick is conducted. Given the mean vector  $\boldsymbol{\mu}$  and the variance matrix  $\boldsymbol{\sigma}$ , we first sample the noise  $\boldsymbol{\epsilon} \sim \mathcal{N}(\mathbf{0}, \mathbf{I})$ . Then the point of joint latent distribution can be computed as  $\mathbf{z} = \boldsymbol{\epsilon}\boldsymbol{\mu} + \boldsymbol{\sigma}$ .

**Attention Module** Considering that certain parts of the features extracted by the model may be useless to the pose regression, we would like to enable our framework to focus on certain representations that are useful to the task, and hence improve the generalization capacity of the model. We implement the non-local style self-attention module [36] in our attention module, which can capture the long-range dependencies and global correlation of the image features [35]. The computation process of attention module can be summarized as following two steps. Give a feature vector  $\mathbf{z} \in \mathbb{R}^D$ , we firstly calculate its self-attention as follow:

$$\mathbf{a} = \text{Softmax}(\mathbf{z}^T \mathbf{W}_\theta^T \mathbf{W}_\phi \mathbf{z}) \mathbf{W}_g \mathbf{z}, \quad (14)$$

where  $\mathbf{W}_\theta$ ,  $\mathbf{W}_\phi$  and  $\mathbf{W}_g$  are the learn-able weights. Then, the residual connection will be added to the linear embedding of the self-attention vectors:

$$\text{Att}(\mathbf{z}) = \alpha(\mathbf{a}) + \mathbf{z}, \quad (15)$$

where the  $\alpha(\mathbf{a}) = \mathbf{W}_\alpha \mathbf{a}$  and the  $\mathbf{W}_\alpha$  is a learnable weight which will be optimized during the training process.

**Pose Regressor** Finally, the re-weighted latent vector is taken as input into the pose regressor to estimate 6-DoF pose. The pose regressor consists of two

parallel networks sharing the same structure. Each network contains two successive fully connected layers connected by a ReLU activation function. Among them, one network predicts the position vector  $\mathbf{p}$ , while another layer predicts the quaternion based rotation vector  $\mathbf{q}$ , which will be used as the final pose estimation.

**Training** During the training process, instead of directly optimizing the whole model together which largely slows down the convergence speed, our training process includes two steps. Firstly, we optimize the model via the loss function without the KL divergence part. Correspondingly, in this step, there is no sampling process for the latent distribution and the mean of the distribution is directly used in the following steps. In the second step, we fixed the learnable weights in the regression loss function and training the rest of the model together.

**Table 1.** The training set and testing set separation of Oxford Robot Car dataset. The route length of LOOP is 1120m and the route length of FULL is 9562m.

Scene	Time	Tag	Training	Testing
-	2014 - 06 - 26 - 08 - 53 - 56	overcast	✓	
-	2014 - 06 - 26 - 09 - 24 - 58	overcast	✓	
LOOP1	2014 - 06 - 23 - 15 - 41 - 25	sunny		✓
LOOP2	2014 - 06 - 23 - 15 - 36 - 04	sunny		✓
-	2014 - 11 - 28 - 12 - 07 - 13	overcast	✓	
-	2014 - 12 - 02 - 15 - 30 - 08	overcast	✓	
FULL1	2014 - 12 - 09 - 13 - 21 - 02	overcast		✓
FULL2	2014 - 12 - 12 - 10 - 45 - 15	overcast		✓

## 4 Experiments

### 4.1 Datasets

Our proposed MVLoc framework is evaluated on two common public datasets: 7-Scenes [30] and Oxford RobotCar [24].

**7-Scenes Dataset** was collected by a Kinect device, consisting of RGB-D image sequences from seven indoor scenarios. The ground truth was calculated by KinectFusion algorithm. Each scene contains several sequences and each sequence usually has 500 or 1000 frames. All the RGB-D images are with a resolution of  $640 \times 480$  pixels. We split the data as training and testing set according to the official instruction.

**Oxford RobotCar Dataset** contains multimodal data from car-mounted sensors, e.g. cameras, LIDAR, and GPS/IMU. The data was recorded under various weather conditions, e.g., heavy rain, night, direct sunlight and snow. In order to make the fair comparison, we use the same data split of this dataset

**Table 2.** The camera localization Results with 7-Scenes Dataset and Oxford RobotCar Dataset. We report the median error of the position and orientation in each case. PoseNet, MapNet and Atloc are based on RGB image only (V), while our MVLoc and VidLoc use RGB and depth maps.

Scene	PoseNet(V)	VidLoc(V,D)	MapNet(V)	AtLoc(V)	MVLoc(V,D)
Chess	0.32m, 6.60°	0.16m, NA	0.08m, 3.25°	0.10m, 4.07°	<b>0.10m, 3.70°</b>
Fire	0.47m, 14.0°	0.19m, NA	0.27m, 11.7°	0.25m, 11.4°	<b>0.25m, 10.5°</b>
Heads	0.30m, 12.2°	0.13m, NA	0.18m, 13.2°	0.16m, 11.8°	<b>0.15m, 10.8°</b>
Office	0.48m, 7.24°	0.24m, NA	0.17m, 5.15°	0.17m, 5.34°	<b>0.16m, 5.08°</b>
Pumpkin	0.49m, 8.12°	0.33m, NA	0.22m, 4.02°	0.21m, 4.37°	<b>0.20m, 4.01°</b>
Red Kitchen	0.58m, 8.34°	0.28m, NA	0.23m, 4.93°	0.23m, 5.42°	<b>0.21m, 5.01°</b>
Stairs	0.48m, 13.1°	0.24m, NA	0.30m, 12.1°	0.26m, 10.5°	<b>0.24m, 10.0°</b>
Average	0.45m, 9.94°	0.23m, NA	0.21m, 7.77°	0.20m, 7.56°	<b>0.19m, 7.01°</b>
LOOP1	-	-	8.76m, 3.46°	8.61m, 4.58°	<b>7.70m, 3.23°</b>
LOOP2	-	-	9.84m, 3.96°	8.86m, 4.67°	<b>7.76m, 3.16°</b>
FULL1	-	-	41.4m, 12.5°	29.6m, 12.4°	<b>24.5m, 4.29°</b>
FULL2	-	-	59.3m, 14.8°	48.2m, 11.1°	<b>42.6m, 8.71°</b>
Average	-	-	29.8m, 8.68°	23.8m, 8.19°	<b>20.6m, 4.85°</b>

named LOOP and FULL as in [4] and [35]. By testing the model in more challenging scenes, the robustness of our model can be fairly proved. As there is no depth map in the original Oxford Robot Car dataset, the depth map is obtained by projecting the sparse LIDAR to the RGB image, while for this depth map, different colors represent the depth of each point as shown in Figure 2. The details of new LOOP and new FULL are shown in Table 1.

## 4.2 Training Details

Our approach is implemented above the PyTorch platform, and trained and tested with an NVIDIA Titan V GPU. During the training process, both RGB images and depth maps are taken as the input, which are rescaled with the shortest side in the length of 256 pixels and normalized into the range of  $[-1, 1]$ . In the case of MVLoc, the sampling number  $k$  is set to be 20. The batch size is set to be 64 and the Adam optimizer is used in the optimization process with the learning rate  $5 \times 10^{-5}$  and the weight decay rate  $5 \times 10^{-5}$ . The training dropout rate is set to be 0.5 and the initialization balance weights are  $\beta_0 = -3.0$  and  $\gamma_0 = 0.0$ .

## 4.3 Baseline and Ablation Study

We take four representative models, i.e. PoseNet [19], VidLoc [9], MapNet [4] and AtLoc [35] as our baselines for a comparison with our proposed method. AtLoc reported the state-of-the-art performance in the 7-scenes and Oxford RobotCar

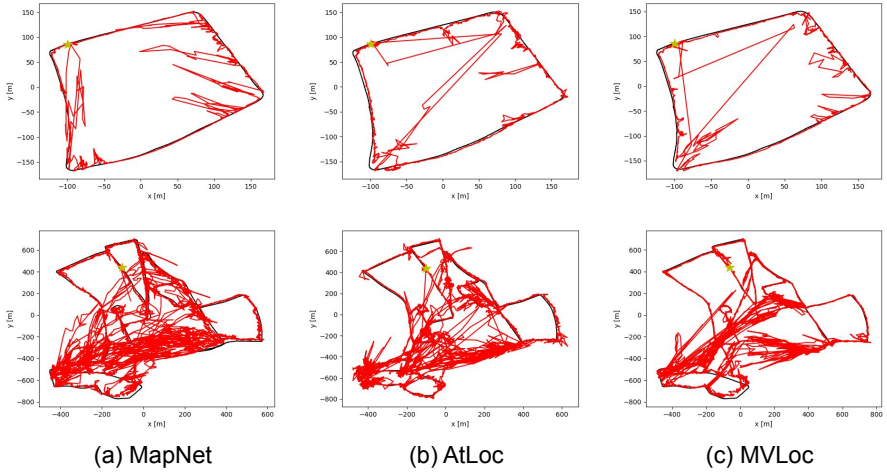


**Fig. 3.** The generated trajectories of LOOP1(Top) and FULL1(Bottom) on the Oxford RobotCar dataset. We compare our proposed (c) MVLoc with two baselines (a) MapNet and (b) AtLoc. The yellow star denotes the starting point. The ground truth trajectories are shown in black lines, while the red lines are the predicted trajectories.

datasets. MapNet uses a sequence of images for re-localization which generally performs better than single image relocalization, and we take it into consideration to prove the high accuracy archived by our single image relocalization algorithm.

To illustrate the effectiveness of each module in our MVLoc framework, we also conducted an ablation study, and compare MVLoc with its three variants: MVLoc (V) denotes a model that uses only RGB images; MVLoc (C) fuses different modalities by concatenating them instead of using our variational method; MVLoc (P) uses the MVAE fusion method without our introduced importance weighting technique.

#### 4.4 The Performance of Proposed MVLoc in Indoor Scenarios

We first evaluate our model on the 7-Scenes dataset to demonstrate its effectiveness in fusing RGB and depth data in indoor scenarios. Table 2 shows the comparison between MVLoc and four representative baselines, PoseNet [19], VidLoc [9], MapNet [4] and AtLoc [35]. The results are reported in the median error (m). MVLoc and VidLoc use both RGB images and depth data, while others are based on RGB images only. Our proposed MVLoc outperforms the other four baseline algorithms in terms of both the position and orientation error. Compared with AtLoc, the previous state-of-the-art method based on a single image, our MVLoc shows a 5.0% improvement upon the position accuracy and a 7.3% improvement in the rotation. Especially, our MVLoc outperforms other

**Table 3.** The ablation study for the performance of MVLoc on Oxford Robot Car Dataset. The MVLoc is compared with the AtLoc (Only using the RGB image) and the MVLoc (MVLoc without the variational fusion method).

Scene	MVLoc (V)	MVLoc (C)	MVLoc (P)	MVLoc
Chess	0.12m, 4.09°	0.10m, 3.85°	0.11m, 4.03°	<b>0.10m, 3.70°</b>
Fire	0.26m, 11.3°	0.25m, 11.0°	0.25m, 11.8°	<b>0.25m, 10.5°</b>
Heads	0.17m, 12.8°	0.16m, 11.0°	0.17m, 10.8°	<b>0.15m, 10.8°</b>
Office	0.18m, 5.44°	0.17m, 5.24°	0.19m, 5.34°	<b>0.16m, 5.08°</b>
Pumpkin	0.21m, 5.47°	0.21m, 4.15°	0.21m, 3.94°	<b>0.20m, 4.01°</b>
Red Kitchen	0.25m, 6.02°	0.23m, 5.25°	0.24m, 5.35°	<b>0.21m, 5.01°</b>
Stairs	0.26m, 10.3°	0.26m, 10.3°	0.26m, 12.0°	<b>0.24m, 10.0°</b>
Average	0.21m, 7.92°	0.20m, 7.26°	0.20m, 7.61°	<b>0.19m, 7.01°</b>
LOOP1	8.61m, 4.58°	8.46m, 3.88°	8.52m, 4.06°	<b>7.70m, 3.23°</b>
LOOP2	8.86m, 4.67°	8.29m, 3.58°	8.27m, 3.75°	<b>7.76m, 3.16°</b>
FULL1	29.6m, 12.4°	26.2m, 10.8°	26.1m, 11.5°	<b>24.5m, 4.29°</b>
FULL2	48.2m, 11.1°	46.5m, 10.1°	45.9m, 10.5°	<b>42.6m, 8.71°</b>
Average	23.8m, 8.19°	22.3m, 7.09°	22.2m, 7.45°	<b>20.6m, 4.85°</b>

algorithms significantly in the Stairs scenario: MVLoc reduces the position error from 0.26m to 0.24m and the rotation error from 10.5° to 10.0°. This may be because Stairs is the highly texture-repetitive scenario and the structure information captured by the depth map can largely help to improve the performance. The improvements made in this case match our expectation and are mainly because of the introduction of depth maps which provide external information for the pose estimation.

To objectively prove the performance of our fusion method, the results of four MVLoc variants on the 7Scenes dataset are shown in the upper part of Table 3. We can notice that all three fusion algorithms perform better than the algorithms only based on a single RGB image, which is consistent with our analysis above. MVLoc (C) has similar performance as MVLoc (P) and both of them perform worse than MVLoc. MVLoc (C) directly concatenate the feature of RGB images and the feature of depth maps together without considering their complementary features. MVLoc (P) implements the simple VAE training strategy whose modeling capability is limited compared with our method.

#### 4.5 Performance of MVLoc in the Driving Scenario

We further evaluate our models on the Oxford RobotCar outdoor dataset. The second part of Table 2 summarizes the performance of two baseline algorithms, MapNet and AtLoc, and the performance of MVLoc. Compared with the AtLoc, MVLoc makes a 13.4% improvement in position accuracy and a 40.8% improvement in rotation accuracy. We can notice that the huge improvement is made in rotation accuracy on four scenes, as the Projection of Point Cloud can capture the structural information of the scene which can largely reduce the rotation er-

ror. While the improvements in the position accuracy are less evident than that in rotation accuracy, the main reason may be that the pointcloud in the Oxford RobotCar dataset is relatively sparse which can only provide limited geometric information. Further improvement can be made when a more powerful modality is added. The visualization for the trajectories of MapNet, AtLoc, and MVLoc for LOOP1 and FULL1 are shown in Figure 3. MVLoc provides a smoother trajectory than MapNet and AtLoc, and predicted trajectory can better fit the ground truth.

The second part of Table 3 presents the ablation studies conducted on Oxford Robot Car Dataset. Compared with the comparison on 7Scenes dataset, MVLoc makes an even larger improvement on the RobotCar Dataset where the environment is even more diverse, as the observation in this dataset may encounter the over-exposure, the changing weather, and dynamic objects. The performance of MVLoc in challenging dataset FULL2 strongly proves that MVLoc can provide a more robust fusion method in complicated circumstances.

**Table 4.** The ablation study for the performance of MVLoc on 7 Scenes Dataset and Oxford Robot Car Dataset in terms of robustness. Here we compare the performance of the MVLoc (V), MVLoc (C) and MVLoc in the condition where the LIDAR data is missing and we replace it with the blank image.

Scene	MVLoc (C)	MVLoc (P)	MVLoc
LOOP1	9.78m, 5.68°	9.9m, 5.81°	<b>8.89m, 4.63°</b>
LOOP2	9.60m, 5.89°	10.3m, 5.97°	<b>8.91m, 4.94°</b>
FULL1	31.9m, 13.5°	31.8m, 15.6°	<b>28.1m, 9.05°</b>
FULL2	51.4m, 13.4°	52.3m, 15.9°	<b>45.1m, 4.66°</b>
Average	25.7m, 9.62°	26.1m, 10.8°	<b>21.7m, 5.82°</b>

## 4.6 The Robustness Evaluation

To indicate the robustness of MVLoc in the case of missing input, we test our models in the condition where the depth maps are missing, and compare its performance with two other fusion strategies including MVLoc (C) and MVLoc (P). MVLoc (C) directly concatenates the feature vectors of RGB image and depth image and put this feature vector to the following module. MVLoc (P) fuses two feature vectors with the PoE, while it optimizes the network with standard VAE objective function.

In this experiment, instead of directly using both RGB images and depth maps for testing, we only input the RGB image for testing and the depth map is replaced by a blank image. The results of this experiment are shown in Table 4. MVLoc outperforms both MVLoc (C) and MVLoc (P). Compared with MVLoc (C) which performs better than MVLoc (P), MVLoc makes a 16.6% improvement in position accuracy and a 39.5% improvement in rotation accuracy. And the

advantages of MVLoc is more evident in the challenging datasets like FULL1 and FULL2. Thus our proposed MVLoc is more robust to perturbations (i.e. missing modalities in this case) compared with other fusion strategies.

## 5 Conclusion

Effectively exploiting multimodal data for localization is a challenging problem, due to the huge difference among various sensor modalities. In this work, we propose a novel multimodal localization framework based on multimodal variational learning. We introduce the importance weighting strategies and geometric-aware learning into the framework to improve the model capacity. Our model achieves the state-of-the-art performance in both indoor and outdoor scenarios. Moreover, the proposed MVLoc also provides a desirable result in the condition when certain inputs are missing.

## References

1. Bijelic, M., Mannan, F., Gruber, T., Ritter, W., Dietmayer, K., Heide, F.: Seeing through fog without seeing fog: Deep sensor fusion in the absence of labeled training data. *arXiv preprint arXiv:1902.08913* (2019)
2. Biswas, J., Veloso, M.: Multi-sensor mobile robot localization for diverse environments. In: *Robot Soccer World Cup*. pp. 468–479. Springer (2013)
3. Brachman, R.J., Schmolze, J.G.: An overview of the KL-ONE knowledge representation system. *Cognitive Science* **9**(2), 171–216 (April–June 1985)
4. Brahmabhatt, S., Gu, J., Kim, K., Hays, J., Kautz, J.: Geometry-aware learning of maps for camera localization. In: *Proceedings of the IEEE Conference on Computer Vision and Pattern Recognition*. pp. 2616–2625 (2018)
5. Burda, Y., Grosse, R., Salakhutdinov, R.: Importance weighted autoencoders. *arXiv preprint arXiv:1509.00519* (2015)
6. Chen, C., Rosa, S., Miao, Y., Lu, C.X., Wu, W., Markham, A., Trigoni, N.: Selective sensor fusion for neural visual-inertial odometry. In: *Proceedings of the IEEE Conference on Computer Vision and Pattern Recognition*. pp. 10542–10551 (2019)
7. Chen, D.M., Baatz, G., Köser, K., Tsai, S.S., Vedantham, R., Pylvänäinen, T., Roimela, K., Chen, X., Bach, J., Pollefeys, M., et al.: City-scale landmark identification on mobile devices. In: *CVPR 2011*. pp. 737–744. IEEE (2011)
8. Chen, X., Ma, H., Wan, J., Li, B., Xia, T.: Multi-view 3d object detection network for autonomous driving. In: *Proceedings of the IEEE Conference on Computer Vision and Pattern Recognition*. pp. 1907–1915 (2017)
9. Clark, R., Wang, S., Markham, A., Trigoni, N., Wen, H.: Vidloc: A deep spatio-temporal model for 6-dof video-clip relocalization. In: *Proceedings of the IEEE Conference on Computer Vision and Pattern Recognition*. pp. 6856–6864 (2017)
10. Clark, R., Wang, S., Wen, H., Markham, A., Trigoni, N.: Vinet: Visual-inertial odometry as a sequence-to-sequence learning problem. In: *Thirty-First AAAI Conference on Artificial Intelligence* (2017)
11. Guzman-Rivera, A., Kohli, P., Glocker, B., Shotton, J., Sharp, T., Fitzgibbon, A., Izadi, S.: Multi-output learning for camera relocalization. In: *Proceedings of the IEEE Conference on Computer Vision and Pattern Recognition*. pp. 1114–1121 (2014)
12. He, K., Zhang, X., Ren, S., Sun, J.: Deep residual learning for image recognition. In: *Proceedings of the IEEE conference on computer vision and pattern recognition*. pp. 770–778 (2016)
13. Higgins, I., Matthey, L., Pal, A., Burgess, C., Glorot, X., Botvinick, M., Mohamed, S., Lerchner, A.: beta-vae: Learning basic visual concepts with a constrained variational framework. *Iclr* **2**(5), 6 (2017)
14. Higgins, I., Sonnerat, N., Matthey, L., Pal, A., Burgess, C.P., Bosnjak, M., Shanan, M., Botvinick, M., Hassabis, D., Lerchner, A.: Scan: Learning hierarchical compositional visual concepts. *arXiv preprint arXiv:1707.03389* (2017)
15. Hinton, G.E.: Products of experts (1999)
16. Kendall, A., Cipolla, R.: Modelling uncertainty in deep learning for camera relocalization. In: *2016 IEEE international conference on Robotics and Automation (ICRA)*. pp. 4762–4769. IEEE (2016)
17. Kendall, A., Cipolla, R.: Geometric loss functions for camera pose regression with deep learning. In: *Proceedings of the IEEE Conference on Computer Vision and Pattern Recognition*. pp. 5974–5983 (2017)



18. Kendall, A., Grimes, M., Cipolla, R.: Convolutional networks for real-time 6-dof camera relocation. *corr abs/1505.07427* (2015) (2015)
19. Kendall, A., Grimes, M., Cipolla, R.: Posenet: A convolutional network for real-time 6-dof camera relocation. In: *Proceedings of the IEEE international conference on computer vision*. pp. 2938–2946 (2015)
20. Kingma, D.P., Welling, M.: Auto-encoding variational bayes. *arXiv preprint arXiv:1312.6114* (2013)
21. Krispel, G., Opitz, M., Waltner, G., Possegger, H., Bischof, H.: Fuseseg: Lidar point cloud segmentation fusing multi-modal data. In: *The IEEE Winter Conference on Applications of Computer Vision*. pp. 1874–1883 (2020)
22. LeCun, Y., Bottou, L., Bengio, Y., Haffner, P.: Gradient-based learning applied to document recognition. *Proceedings of the IEEE* **86**(11), 2278–2324 (1998)
23. Liang, M., Yang, B., Chen, Y., Hu, R., Urtasun, R.: Multi-task multi-sensor fusion for 3d object detection. In: *Proceedings of the IEEE Conference on Computer Vision and Pattern Recognition*. pp. 7345–7353 (2019)
24. Maddern, W., Pascoe, G., Linegar, C., Newman, P.: 1 year, 1000 km: The oxford robotcar dataset. *The International Journal of Robotics Research* **36**(1), 3–15 (2017)
25. Melekhov, I., Ylioinas, J., Kannala, J., Rahtu, E.: Image-based localization using hourglass networks. In: *Proceedings of the IEEE International Conference on Computer Vision*. pp. 879–886 (2017)
26. Qi, C.R., Liu, W., Wu, C., Su, H., Guibas, L.J.: Frustum pointnets for 3d object detection from rgb-d data. In: *Proceedings of the IEEE Conference on Computer Vision and Pattern Recognition*. pp. 918–927 (2018)
27. Radwan, N., Valada, A., Burgard, W.: Vlocnet++: Deep multitask learning for semantic visual localization and odometry. *IEEE Robotics and Automation Letters* **3**(4), 4407–4414 (2018)
28. Rainforth, T., Kosiorek, A.R., Le, T.A., Maddison, C.J., Igl, M., Wood, F., Teh, Y.W.: Tighter variational bounds are not necessarily better. *arXiv preprint arXiv:1802.04537* (2018)
29. Shi, Y., Siddharth, N., Paige, B., Torr, P.: Variational mixture-of-experts autoencoders for multi-modal deep generative models. In: *Advances in Neural Information Processing Systems*. pp. 15692–15703 (2019)
30. Shotton, J., Glocker, B., Zach, C., Izadi, S., Criminisi, A., Fitzgibbon, A.: Scene coordinate regression forests for camera relocation in rgb-d images. In: *Proceedings of the IEEE Conference on Computer Vision and Pattern Recognition*. pp. 2930–2937 (2013)
31. Suzuki, M., Nakayama, K., Matsuo, Y.: Joint multimodal learning with deep generative models. *arXiv preprint arXiv:1611.01891* (2016)
32. Tucker, G., Lawson, D., Gu, S., Maddison, C.J.: Doubly reparameterized gradient estimators for monte carlo objectives. *arXiv preprint arXiv:1810.04152* (2018)
33. Van Steenkiste, T., Deschrijver, D., Dhaene, T.: Sensor fusion using backward shortcut connections for sleep apnea detection in multi-modal data. *arXiv preprint arXiv:1912.06879* (2019)
34. Walch, F., Hazirbas, C., Leal-Taixe, L., Sattler, T., Hilsenbeck, S., Cremers, D.: Image-based localization using lstms for structured feature correlation. In: *Proceedings of the IEEE International Conference on Computer Vision*. pp. 627–637 (2017)
35. Wang, B., Chen, C., Lu, C.X., Zhao, P., Trigoni, N., Markham, A.: Atloc: Attention guided camera localization. *arXiv preprint arXiv:1909.03557* (2019)

36. Wang, X., Girshick, R., Gupta, A., He, K.: Non-local neural networks. In: Proceedings of the IEEE Conference on Computer Vision and Pattern Recognition. pp. 7794–7803 (2018)
37. Wu, M., Goodman, N.: Multimodal generative models for scalable weakly-supervised learning. In: Advances in Neural Information Processing Systems. pp. 5575–5585 (2018)
38. Xiao, H., Rasul, K., Vollgraf, R.: Fashion-mnist: a novel image dataset for benchmarking machine learning algorithms. arXiv preprint arXiv:1708.07747 (2017)
39. Yang, L., Li, S., Lee, D., Yao, A.: Aligning latent spaces for 3d hand pose estimation. In: Proceedings of the IEEE International Conference on Computer Vision. pp. 2335–2343 (2019)
40. Zeisl, B., Sattler, T., Pollefeys, M.: Camera pose voting for large-scale image-based localization. In: Proceedings of the IEEE International Conference on Computer Vision. pp. 2704–2712 (2015)